MODELLING AND EXPERIMENTAL STUDIES OF A X-BAND WINDOW FOR MOBILE LINACS*

Y. Rozier†, Epsyl, Pertuis, France
M. Boucard, AVELION, Peynier, France

Abstract

Radio-frequency (RF) windows are sensitive components that ensure both RF power transmission and vacuum integrity in linear accelerators (LINACs). In the X-band frequency, improving reliability is critical for compact LINAC systems, including application in non-destructive testing and medical technologies.

This study presents an RF window designed for operation at 9.3 GHz with a 2.0 MW peak-power design target. This window is optimised to reduce peak electric field at the ceramic–metal brazed interface while preserving low insertion loss and broad bandwidth. Coupled RF–fluidic–thermal simulations guided an extended cylindrical pillbox design exploiting the TE_{112} mode.

A prototype has been fabricated, and low-power RF measurements have been carried out to validate both the design and manufacturing process. RF simulations and low-power tests show insertion losses below 0.1 dB and a standing-wave ratio lower than 1.05 at 9.3 GHz. High-power endurance tests carried out on the prototype demonstrated stable behaviour.

Results of the engineering design will be compared with tests and discussed.

INTRODUCTION

High-gradient X-band LINACs require robust and low-loss RF windows that reliably transmit high peak power while ensuring vacuum integrity. The main design objectives are therefore to suppress unwanted mode conversion, avoid resonant ghost modes and, minimize peak electric field in the designed component. Achieving these goals demands solutions that go beyond a simple pill-box design [1] for field considerations. Integration of iris in waveguide [2], progressive taper [3] or over-sized dimensions [4] approaches leads to dimensional constraints on the final system. Mixed-mode designs [5, 6] have also been reported in the literature.

The RF window presented in this study is designed to operate at a peak power level of 2.0 MW with a pulse length t_P of 5.0 µs. The technical requirements are further constrained by the need to minimize heating of the component and running in an ultra-high vacuum ($P < 5 \times 10^{-9}$ mbar). The full set of specifications for this window developed for our new accelerator section [7] is provided in Table 1.

The simultaneous requirements of mechanical compactness and ultra-high vacuum operation in the LINAC impose significant design constraints. In particular, the reduction of the RF field must be achieved without compromising insertion loss or bandwidth performance. Given the limited availability of commercial devices operating near the target frequency of f_C = 9.3 GHz, the development of a dedicated solution is therefore required to meet these specifications.

Table 1: RF window specification

Item	Value	Unit
Central frequency f_C	9.3	GHz
RF peak power	2.0	MW
Pulse length t_P	5.0	µs
RF average power	1.6	kW
RF bandwidth	> 50	MHz
Reflection S_{ii}	< −19.1	dB
Transmission S_{ij}	< 0.2	dB
Pressure withstanding	3.0	bar abs.

ENGINEERING DESIGN

Process Considerations

The RF window includes a customised choke with a DN40CF vacuum flange on the LINAC side and a WR90 square cover flange on the external side. The component is manufactured using a two-stage brazed approach. A 97.6 % vacuum grade Al_2O_3 (AL300®, Morgan Advanced Ceramics) has been used for this purpose. Its relative permittivity is 9.04 at 8.5 GHz, which is consistent with the operating frequency range. During assembly, particular attention is given to the alignment of both flanges (< 1.0 ° deviation) to minimise the contribution of a ghost mode at 8.895 GHz. The manufacturing drawing of the RF window is shown in Fig. 1. Cooling pipes (not shown here) are subsequently integrated with tailored orientations and terminations to comply with the environmental and operational constraints of the complete system.

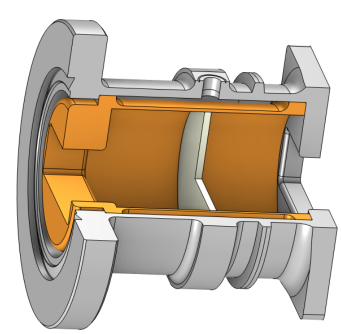

Figure 1: Mechanical design of the RF window.

* This work was supported by a grant from the French Public Investment Bank (Bpifrance) as part of the France 2030 program.

† yrozier@avelion-alcen.com

Coupled Modelling

Numerical simulations were performed using Comsol Multiphysics®, coupling several physics: RF, heat transfer, laminar flow and structural mechanics. The RF design has been performed to ensure the best transmission possible along the entire structure path, starting from the choke flange up to the pillbox window. However, due to the compact diameter of the ceramic, the simple pillbox design approach does not provide optimal performances with respect to the geometrical constraints of the X-band. The alternative approach is to extend the cylinder length to exploit the TE_{112} longitudinal mode. This approach leads to a significant reduction of the ceramic surface fields in the optimized design.

Electromagnetic simulations were carried out for a 2.0 MW peak RF field. The simulations yield a surface electric field of 0.90 kV/mm and a surface magnetic field of 6.15 A/mm at the ceramic window; these values are minimized by the TE_{112} longitudinal mode (Fig. 2).

These field levels provide increased tolerance with respect to potential brazing excess during fabrication. The maximum electrical field observed (6.94 kV/mm) is located at half the length of the rectangular-circular transition. This value is below the design limit (< 10 kV/mm) and could be further reduced through appropriate edge rounding. The main drawback of an extended cylindrical window could be the presence of nearby RF modes. These modes are located 189.8 MHz below and 131.0 MHz above the central frequency f_C. They are sufficiently far away from the ±25 MHz oscillating band of the magnetron, excluding any interference during the experimental runs.

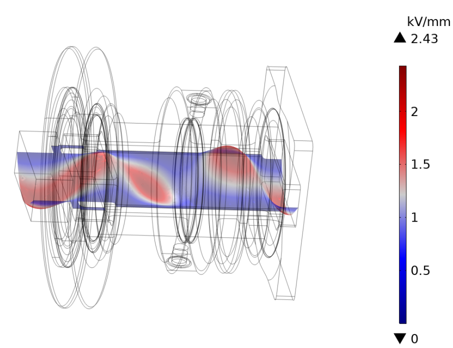

Figure 2: Simulated electric field for 2.0 MW, 9.3 GHz.

Additional multiphysics simulations were conducted under steady state conditions, incorporating thermal analysis, fluid flow, and structural deformation. These simulations have been performed at an average transmitted RF power of 1.6 kW, which corresponds to the maximum possible average power delivered by the available magnetrons. The cooling principle is very simple, with water injected at 25 °C under a flow rate of 4.0 L/min and an inlet pressure of 4.0 bar. Maximum Reynolds number Re monitored is 1217, below the turbulent limit of $Re = 2300$. The coolant velocity ranges from 0.25 m/s to 7.1 m/s within the cooling jacket and reaches 9.2 m/s at the pipe inlet. Temperature increase is limited to $\delta T = 1.2$ °C on metallic parts and $\delta T = 0.02$ °C on the Al_2O_3 ceramic. These results indicate comfortable thermal margins and suggest potential for further simplification of the cooling system. Results are illustrated in Fig. 3.

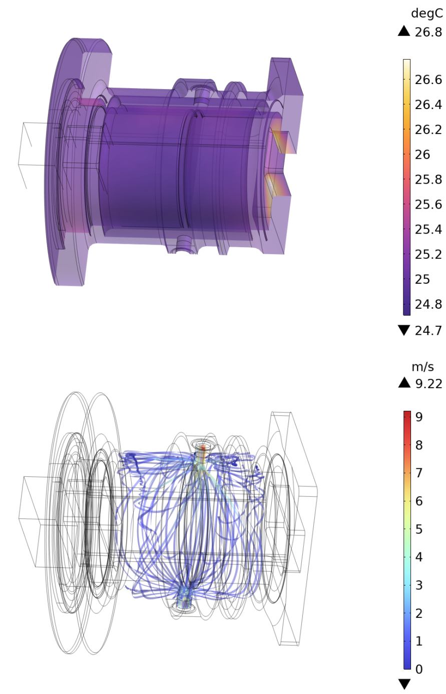

Figure 3: Simulated thermal field (top) and water flow (bottom) maps for an average RF power of 1.6 kW.

EXPERIMENTAL VALIDATION

Low-Power Tests

After the brazing sequence, helium leak tightness has been measured to 4×10^{-10} mbar L/s, confirming compatibility with ultra-high vacuum operation. Low-power measurements have been carried in air (19.9 °C and 44 % relative humidity) on both side of the window. RF transmission ($S_{12} = -0.07$ dB) and reflection ($S_{11} = -26.4$ dB) have been measured at the central frequency. The measured response across the magnetron bandwidth are plotted alongside the initial modelling conditions (Fig. 4). These measurements are compared to several modelling scenarios: vacuum ($\epsilon_r = 1.0$), air ($\epsilon_r = 1.0029$ for 19.9 °C and 44 % relative humidity) or SF_6 gas ($\epsilon_r = 1.0021$). The measurements indicate noticeable discrepancies with the initial model, as shown in Fig. 4.

The sole change of the dielectric medium in the modelling conditions, from pure vacuum to realistic air, only partially reduces the differences between simulation and measurement and does not fully account for the observed deviations. The present model underestimate the damping observed experimentally. Higher dielectric losses in Al_2O_3 should minimize discrepancies. In addition, incorporation of the exact geometric dimensions, alignments, and precise volume of the brazing joint could give a more accurate description.

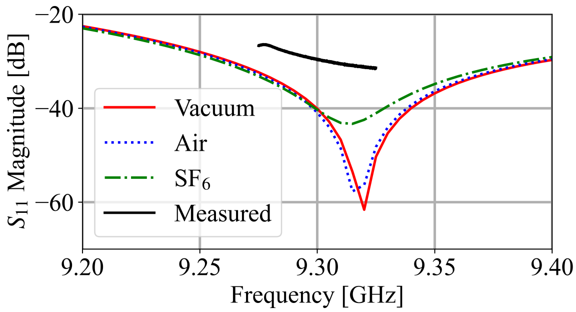

Figure 4: Simulated and measured reflected RF power S_{11}.

High-Power RF Tests

The high-power tests of the window were performed in a configuration representative of the LINAC environment. The experimental setup is shown in Fig. 5. A 1.75 MW peak power (t_P=4.6 µs, 200 Hz giving 1.6 kW average power) tuneable magnetron oscillating at 9.3 GHz feeds the RF power in the test bench. The window is placed between a bidirectional coupler (left side of the figure) and a water load (right side of the figure).

To reproduce LINAC operating scenarios, controlled mismatches were intentionally introduced downstream of the RF window. This was implemented designing a symmetric capacitive iris to replicate various coupling coefficient β scenarios. Three representatives conditions were tested:

- β =1, perfect transmission (no iris, no beam)
- β =1.18, low beam loading (iris of S_{11} = −21.7 dB)
- β =1.5, higher beam loading (iris of S_{11} = −14.0 dB)

The transmission line was pressurized on both sides with 2.0 bar absolute of SF_6 to simplify testing procedures and ensure compatibility with components (load, isolator). With this protocol, the observed breakdown thresholds may differ from those expected in a vacuum LINAC environment.

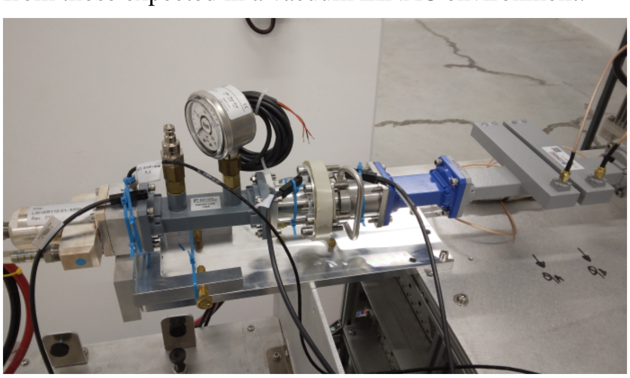

Figure 5: High-Power test bench configuration.

Continuous monitoring of transmitted power, reflected power, and arcs in the magnetron, is performed. During the whole power ramping sequence, no indication of performance degradation has been observed.

At the end of the power ramping sequence, an endurance test at full peak power and full average power is performed for each iris conditions, checking the temperature increase on the outer surface.

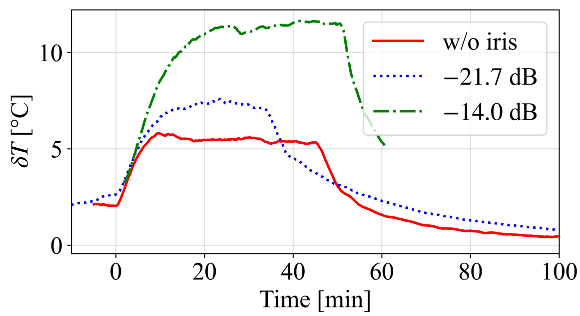

Figure 6: Temperature increase during endurance tests.

The test duration variates from 33 min (S_{11} = −14.0 dB iris) to 50 min (S_{11} = −21.7 dB iris), leading to nearly steady-state conditions after 20 min of application of RF power. The results are summarized in Fig. 6 with a maximum temperature increase of δT = 5.8 °C (no iris), δT = 7.6 °C (S_{11} = −21.7 dB iris) and δT = 11.6 °C (S_{11} = −14.0 dB iris). These temperature rises are consistent with the higher transmission losses measured during the low-power tests. No evidence of arcing or abnormal reflected power transients was observed under any test condition. Post-test measurements confirmed the stability of RF transmission and reflection characteristics, as well as the preservation of helium leak tightness, indicating appropriate design margins for the RF window.

CONCLUSION

A prototype RF window for X-band LINAC working at 9.3 GHz was designed, manufactured, and experimentally validated. The design, based on an extended cylindrical pillbox geometry supporting the TE_{112} mode, was developed using coupled RF, thermal, and fluid simulations. This approach enabled a reduction of peak RF fields at the ceramic–metal interface while maintaining low insertion loss and broad bandwidth performance.

High-power testing up to 1.75 MW peak power and 1.6 kW average power demonstrated stable operation across all tested configurations, including matched conditions and representative beam loading scenarios. No arcing, RF degradation, or loss of vacuum integrity was observed.

The successful completion of the manufacturing and tests will enable future integration into our X-band products.

ACKNOWLEDGMENTS

The authors thank N. Tannoury and T. Campanella for technical supervision, V. Parga and R. Convers for CAD design, J. Sommervogel, J. Marre, and G. Sanz for prototype manufacturing, and G. Folcher for conducting the bunker tests. Their expertise and support were essential to the successful completion of this work.

REFERENCES

[1] A. Leggieri, A. Ciccotelli, and G. Felici, "Tuned Window for Standing Wave Linear Accelerators", *in Proc. Prog. Electromagn. Res. Symp. 2014 (PIERS'14)*, Guangzhou, China, Aug. 2014, pp. 2421–2428. ISBN: 978-1-934142-28-8

[2] A. Jöstingmeier, M. Dohlus, and N. Holtkamp, "Systematic Design of an S-band Pillbox-Type RF Window", *in Proc. LINAC'98*, Chicago, U.S.A., Aug. 1998, paper MO4081, pp. 249–251. https://jacow.org/l98/papers/MO4081.pdf

[3] Y. Otake, S. Tokumoto, and H. Mizuno, "Design and High-Power Test of a TE11-mode X-band RF Window with Taper Transitions", *in Proc. PAC'95*, Dallas, U.S.A., May 1995, paper TAQ29, pp. 1590–1592. doi:10.1109/PAC.1995.505296

[4] W. R. Fowkes, R. S. Callin, and E. N. Jongewaard, "Large diameter reduced field TE01 traveling wave window for X-band", *in Proc. PAC'99*, New York, U.S.A., Mar 1999, paper MOP53, pp. 783–785. doi:10.1109/PAC.1999.795354

[5] S. Kazakov, "Development of New Type of High Power RF Window", Ph.D. thesis, 2003, Dept. of Accelerator Science, The Graduate University for Advanced Studies (Sōkendai), Hayama, Japan, 2003.

[6] B. V. Prokofiev and M. A. Martynenko, "A simple pillbox-type mixed-mode window for high power microwave devices", *in Proc. 18th Int. Vac. Electron. Conf. (IVEC'17)*, London, United Kingdom, April 2017. doi:10.1109/ivec.2017.8289511

[7] M. Boucard and Y. Rozier, "Compact X-Band Linear Accelerators Design for On-Site Industrial Applications", presented at IPAC'26, Deauville, France, May 2026, paper TUP8002, this conference.